Metal clusters that freeze into high energy geometries

Martin F. Jarrold, Baopeng Cao, Anne K. Starace, Colleen M. Neal, and Oscar H. Judd

Citation: The Journal of Chemical Physics **129**, 014503 (2008); doi: 10.1063/1.2939579
View online: http://dx.doi.org/10.1063/1.2939579
View Table of Contents: http://scitation.aip.org/content/aip/journal/jcp/129/1?ver=pdfcov
Published by the AIP Publishing

Metal clusters that freeze into high energy geometries

Martin F. Jarrold,[a] Baopeng Cao, Anne K. Starace, Colleen M. Neal, and Oscar H. Judd
Chemistry Department, Indiana University, 800 East Kirkwood Avenue, Bloomington, Indiana 47405, USA

(Received 29 February 2008; accepted 14 May 2008; published online 1 July 2008)

Heat capacities measured for isolated aluminum clusters show peaks due to melting. For some clusters with around 60 and 80 atoms there is a dip in the heat capacities at a slightly lower temperature than the peak. The dips have been attributed to structural transitions. Here we report studies where the clusters are annealed before the heat capacity is measured. The dips disappear for some clusters, but in many cases they persist, even when the clusters are annealed to well above their melting temperature. This indicates that the dips do not result from badly formed clusters generated during cluster growth, as originally suggested. We develop a simple kinetic model of melting and freezing in a system consisting of one liquidlike and two solidlike states with different melting temperatures and latent heats. Using this model we are able to reproduce the experimental results including the dependence on the annealing conditions. The dips result from freezing into a high energy geometry and then annealing into the thermodynamically preferred solid. The thermodynamically preferred solid has the higher freezing temperature. However, the liquid can bypass freezing into the thermodynamically preferred solid (at high cooling rates) if the higher energy geometry has a larger freezing rate. © *2008 American Institute of Physics*.
[DOI: 10.1063/1.2939579]

INTRODUCTION

The melting of small particles has been studied for many years. It is now almost a century since Pawlow predicted that small particles have depressed melting points.[1] This prediction has now been confirmed for particles with 10^3–10^6 atoms.[2–6] However, it is only recently that experimental studies have been performed for clusters with fewer than 10^3 atoms.[7–13] These studies revealed large size-dependent variations in the melting temperatures and engendered theoretical investigations to understand their origin.[14–26] Most experimental studies of cluster melting have used calorimetry based methods. Here the heat capacity of the cluster is measured as a function of temperature, and a peak in the heat capacity is used to identify the melting transition.

In recent studies of the melting of aluminum cluster cations we found a dip in the heat capacities of clusters with around 60 and 80 atoms, at a slightly lower temperature than the peak.[27,28] We attributed the dip to a structural transition where a badly formed or amorphous cluster generated during cluster growth converts into the ground state as the temperature is raised. Whether or not this explanation is correct can be tested by annealing the clusters before the heat capacity is measured.

In this paper we report the requisite annealing studies. We have incorporated an annealing section between the cluster growth region and where the temperature is set for the heat capacity measurements. The dip disappears for some of the clusters when they are annealed to above their melting temperature, but for many clusters it persists. This indicates that the dips do not result from badly formed clusters generated during cluster growth. Instead, we suggest that the dips result from freezing into a high energy geometry which subsequently anneals into the thermodynamically preferred solid. To investigate this idea, we developed a simple kinetic model with a liquidlike state and two solidlike states with different melting temperatures and latent heats. The model reproduces the annealing behavior observed in the experiments and identifies the conditions for a liquid cluster to preferentially freeze into a high energy geometry.

EXPERIMENTAL METHODS

The apparatus employed for the experimental studies has been described in detail elsewhere.[29] For the measurements reported here an annealing section has been added to the source (see Fig. 1). The 5 cm long annealing section is separated from the cluster growth region and the 10 cm long temperature variable extension by 1 cm thick Macor® spacers. The cluster growth region is held at close to room temperature, and the annealing section and temperature variable extension can be independently varied from 77 to 1200 K. The clusters are generated by pulsed laser vaporization of a liquid metal target in a continuous flow of helium.[30] After formation, the cluster ions are carried through the annealing section and into the temperature-variable extension where their temperature is set for the heat capacity measurements.

Cluster ions that exit the temperature-variable extension are focused into a quadrupole mass spectrometer where a particular cluster size is selected. The size-selected clusters are then focused into a high pressure collision cell containing helium. When the cluster ions enter the collision cell they undergo numerous collisions with the helium collision gas,

[a]Author to whom correspondence should be addressed. Electronic mail: mfj@indiana.edu.

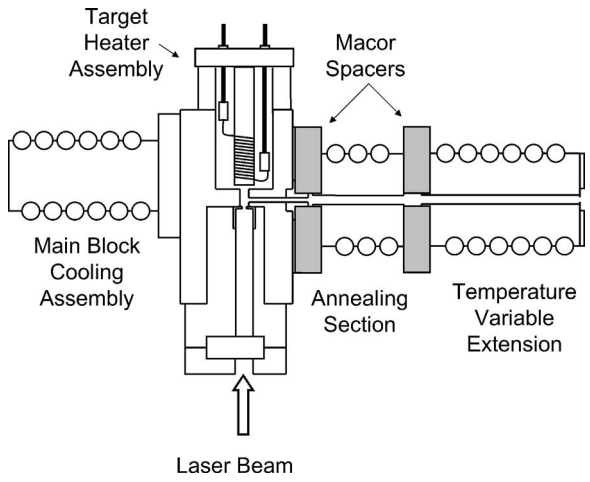

FIG. 1. Schematic diagram of the source showing the annealing section and temperature variable extension used to set the temperature of the clusters.

each one converting a small fraction of the ion's translational energy into internal energy. If their initial translational energy is large enough, some of the clusters are energized to the point where they dissociate. Dissociation occurs by sequential evaporation of aluminum atoms. Fragment ions and undissociated cluster ions are drawn across the collision cell by a weak electric field. At the other side of the collision cell some of the ions exit; these ions are focused into a second quadrupole mass spectrometer where they are mass analyzed and then detected.

The fraction of clusters that dissociate is determined from the mass spectrum, and measured as a function of the ions translational energy at the entrance of the collision cell. The translational energy for 50% of the clusters to dissociate (TE50%D) is then obtained from a linear regression. TE50%D is determined as a function of the extension temperature. The TE50%D values decrease as the temperature is increased because the cluster's internal energy increases. At the melting temperature there is a sharp drop in TE50%D due to the latent heat. The derivative of TE50%D with temperature is proportional to the heat capacity. The proportionality constant is related to the fraction of the cluster ions' kinetic energy that is converted into internal energy as the clusters enter the collision cell. This quantity is obtained from a simple impulsive collision model.[31,32]

EXPERIMENTAL RESULTS

Figure 2 (color online) shows heat capacities measured for $Al_{55}^{+}-Al_{62}^{+}$ and $Al_{80}^{+}-Al_{83}^{+}$. The heat capacities are plotted in terms of the classical value $3Nk_B$ where $3N=3n-6+3/2$ (n is the number of atoms in the cluster) and k_B is the Boltzmann constant. The thin dashed lines in the figure are heat capacities derived from a modified Debye model.[33] The filled black circles are heat capacities measured without the annealing section. These heat capacities show less scatter than our previously reported results[27] because we have performed some more measurements; the new measurements are similar to the old, but averaging over both data sets leads to less scatter. The peaks in the heat capacities, clearly evident in Fig. 2, are due to melting. The areas under the peaks are the latent heats. Many of the clusters also show significant dips in their heat capacities at slightly lower temperatures than the peaks.

The open red squares in Fig. 2 represent heat capacities recorded with the annealing section set to 873 K (which is indicated by the solid vertical lines in Fig. 2). At 873 K, the annealing section is well above the melting temperature of all the clusters shown in Fig. 2, so annealing must involve melting and refreezing. The position and size of the peaks in the heat capacities are virtually unchanged by annealing to 873 K. However, for some cluster sizes the dip disappears. This behavior is most clearly illustrated by clusters with 81 and 82 atoms. For Al_{80}^{+}, the dip in the heat capacity is broader than for the other clusters, but it still largely disap-

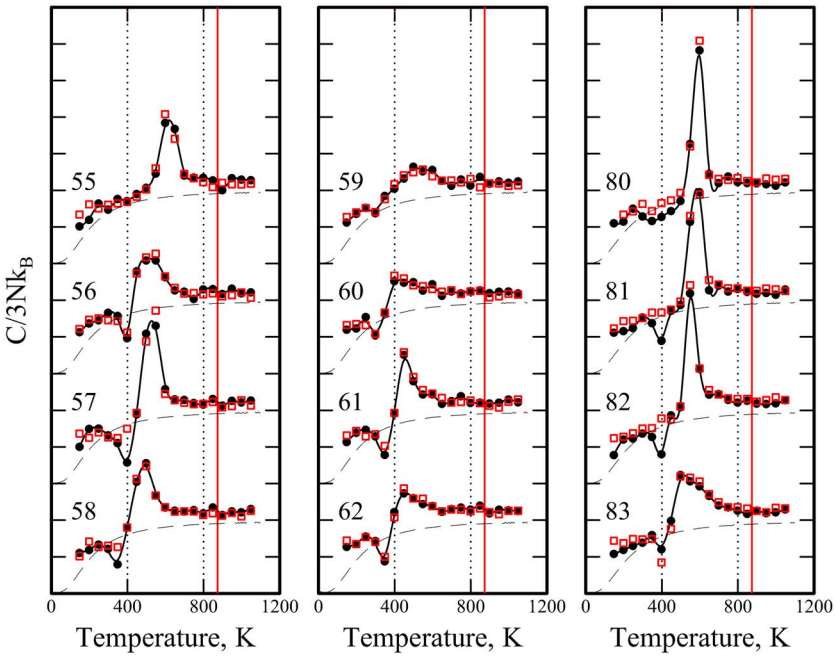

FIG. 2. (Color online) Heat capacities measured for Al_n^+ with $n=55-62$ and 80–83 plotted in terms of the classical value, $3Nk_B$, where $3N=3n-6+3/2$ and k_B is the Boltzmann constant. The thin dashed lines are the heat capacities derived from a modified Debye model (Ref. 33). The filled black circles show results recorded without the annealing section. The solid black line going through the points is a spline fit. The open red squares are heat capacities measured with the annealing section at 873 K. This temperature, shown by the vertical red line, is well above the melting temperatures of all of the clusters in the figure.

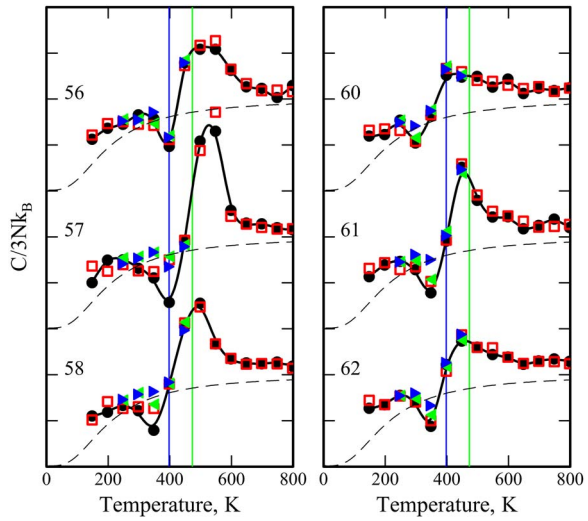

FIG. 3. (Color online) Heat capacities measured for Al_n^+ with $n=56$, 57, 58, 60, 61, and 62 plotted in terms of the classical value, $3Nk_B$, where $3N=3n-6+3/2$ and k_B is the Boltzmann constant. The thin dashed lines are the heat capacities derived from a modified Debye model (Ref. 33). The filled black circles are heat capacities measured without the annealing section. The solid black line is a spline fit. The open red squares are heat capacities recorded with the annealing section at 873 K. The filled green left-pointing triangles represent heat capacities measured with an annealing temperature of 473 K (vertical green line). The filled blue right-pointing triangles show heat capacities recorded with an annealing temperature of 400 K (vertical blue line).

pears when this cluster is annealed to 873 K. For Al_{83}^+, on the other hand, the dip becomes slightly deeper when the clusters are annealed.

Clusters with around 60 atoms also show a variety of behaviors when they are annealed. For Al_{57}^+ the dip essentially disappears, while for Al_{58}^+ and Al_{61}^+ it partially disappears. For all the other clusters that show significant dips (Al_{56}^+, Al_{60}^+, and Al_{62}^+) the dip remains virtually unchanged when the clusters are annealed at 873 K.

Since annealing to 873 K did not remove many of the dips, some measurements were performed with more gentle annealing conditions. The results are presented in Fig. 3. The green left-pointing triangles show the results measured with an annealing temperature of 473 K and the blue right-pointing triangles show results obtained with 400 K. Solid vertical lines show the annealing temperatures. Some of the dips which persist after annealing to 873 K are filled in or partially filled in with the lower annealing temperatures (Al_{58}^+ and Al_{61}^+, for example). However, in other cases (Al_{56}^+, for example) the dip remains unchanged.

In summary then, annealing to well above the melting temperature removes some of the dips, diminishes others, and leaves the rest unchanged. More gentle annealing conditions remove more of the dips, but even with the mildest annealing conditions some of the dips persist.

INITIAL INTERPRETATION OF THE EXPERIMENTAL RESULTS

Cluster growth through the sequential addition of atoms can lead to high energy structures if there is not enough energy or time available for the cluster to rearrange during accretion. If the dips result from amorphous or badly formed geometries generated during cluster growth they should disappear when the clusters are annealed to above their melting temperatures. Many of the dips, however, do not disappear and so we seek another explanation. The fact that the dips persist when the clusters are melted and refrozen suggests that they may result from freezing into a high energy geometry which subsequently anneals into the thermodynamically preferred solid in the temperature variable extension. Some simple models were developed to test this idea.

SIMPLE EQUILIBRIUM AND KINETIC MODELS OF CLUSTER MELTING AND FREEZING

We start by assuming that melting and freezing occurs in the dynamic coexistence regime where the transitions are between fully liquidlike and fully solidlike clusters. This behavior has been observed in computer simulations.[34–37] The absence of partially liquid clusters has been attributed to the relatively high energetic cost of the liquid-solid interface.[36] In macroscopic systems, the cost of the interface is small compared to overall energy of the system and melting and freezing occurs with the two phases in contact. Where the dynamic phase coexistence of small systems switches to the static phase coexistence of macroscopic objects has not been determined experimentally, but simulations suggest hundreds of atoms are required.[38–41]

The minimum ingredients needed to fit the experimental results are two solidlike states and one liquidlike. We assume that both solids can melt into the liquid and that the liquid can freeze into both solids. Transitions between the solids occur through the liquid (i.e., the cluster melts and then freezes into the other structure). This behavior has been observed in computer simulations of Lennard-Jones clusters.[42] We could add a direct solid-to-solid pathway (i.e., one that does not go through the liquid) if our model is found to be inadequate, but as we will see below this is unnecessary. We first consider a model where the three states are in equilibrium. We start here because thermodynamic behavior is expected in the limit of fast melting and freezing. Our equilibrium model is related to the two state model recently described by Poland.[43]

A MODEL BASED ON EQUILIBRIUM

We assume that both solids (S_A and S_B) are in equilibrium with the liquid (L) and that both equilibria are characterized by an equilibrium constant given by

$$K(T)=\exp\left[-\frac{\Delta H_m}{R}\left(\frac{1}{T}-\frac{1}{T_m}\right)\right], \tag{1}$$

where ΔH_m is the latent heat, T_m is the melting temperature, and R is the gas constant. Four parameters define the model: ΔH_m^A, ΔH_m^B, T_m^A, and T_m^B. There are two cases: in the first (case 1) the larger ΔH_m is paired with the smaller T_m; and in the second (case 2) the larger ΔH_m and the larger T_m are paired. Table I gives values for ΔH_m and T_m employed in the simulations. The entropies of melting, given by $\Delta S_m=\Delta H_m/T_m$,

TABLE I. Summary of parameters used in the simulations and the temperature ranges over which the solids are thermodynamically preferred.

	ΔH_m (kJ mol^{-1})	T_m (K)	ΔS_m (J K^{-1} mol^{-1})	Thermodynamically preferred
Case 1				
solid A	150	400	375	0–286 K
solid B	100	500	200	286–500 K
Case 2				
solid A	150	500	300	0–500 K
solid B	100	400	250	

are also given in the table.

The contribution of the latent heats to the internal energy and heat capacity of the three component system (S_A, S_B, and L) are

$$E_{\text{int}}(T) = -f_{SA}(T)\Delta H_m^A - f_{SB}(T)\Delta H_m^B \tag{2}$$

and

$$C(T) = \frac{dE_{\text{int}}}{dT} = \frac{\Delta(-f_{SA}(T)\Delta H_m^A - f_{SB}(T)\Delta H_m^B)}{\Delta T}, \tag{3}$$

where $f_{SA}(T)$ and $f_{SB}(T)$ are the fractions of solids A and B present, respectively.

Figure 4 shows results for the two limiting cases described above: Case 1 on the left and case 2 on the right. The top panels show equilibrium constants for the solid$\rightleftarrows$liquid transitions ($S_A \rightleftarrows L$ and $S_B \rightleftarrows L$) plotted against temperature. The melting transition occurs at $K=1$. The middle panels show the relative abundances of S_A (green line), S_B (blue line), and L (red line). The bottom panels show the component of the heat capacities due to the latent heat determined using Eq. (3).

For case 1 (right side of Fig. 4) solid A dominates at low temperature because it has a larger latent heat. However, as the temperature is raised solid B becomes dominant because it has a higher entropy (a smaller ΔS_m). The transition occurs where the equilibrium constants intersect at 286 K and it leads to a peak in the heat capacity with an area given by $\Delta H_m^A - \Delta H_m^B = 50$ kJ/mol. The larger peak in the heat capacity at ~500 K is due to the melting of solid B. The area under this peak is the latent heat of solid B (100 kJ/mol). There is no peak in the heat capacity for the melting of solid A, because the amount of solid A present at 400 K is very small.

For case 2 (left side of Fig. 4) solid A is the thermodynamically preferred solid at all temperatures below the melting temperature. There is only one peak in the heat capacity due to the melting of solid A at 500 K. The area under this peak is the latent heat (150 kJ/mol).

In both cases, the liquid freezes at the higher melting temperature (500 K) into the solid with the lowest free energy. A solid-to-solid transition occurs below both melting temperatures for case 1, however, this leads to a second peak in the heat capacities, not a dip. Since an equilibrium-based model cannot explain our results, we now explore a model that incorporates the kinetics of melting and freezing.

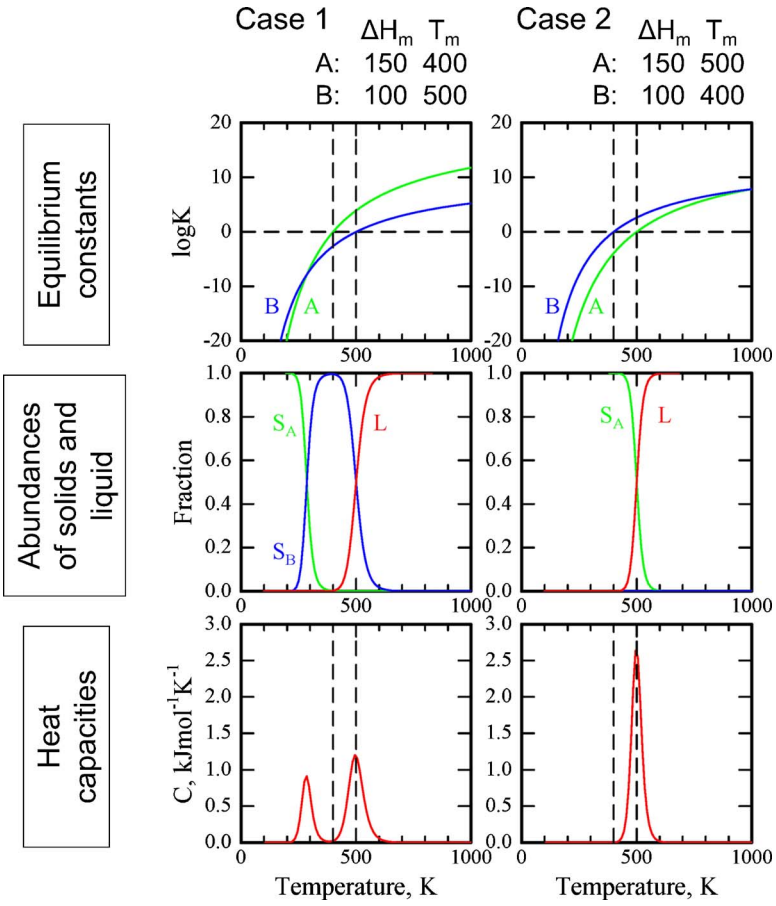

FIG. 4. (Color online) Predictions of the equilibrium model. The panels on the left show results for case 1 and those on the right are for case 2. The top panels show equilibrium constants, $S_A \rightleftarrows L$ (green) and $S_B \rightleftarrows L$ (blue), plotted against temperature. The middle panels show the relative abundance of solid A (green), solid B (blue), and liquid (red) as a function of temperature. The bottom panels show the component of the heat capacities due to the latent heat as a function of temperature.

A MODEL BASED ON KINETICS

To implement a kinetic model, rate constants are required for the melting and freezing of solids A and B. Essentially nothing is known about the melting and freezing rates for metal clusters and so we make some simple assumptions. For melting, we use the Arrhenius expression with the activation energy given by ΔH_m,

$$k_m = Ae^{-E_A/RT} = Ae^{-\Delta H_m/RT}. \quad (4)$$

The rate constant for freezing is then given by

$$k_f = \frac{k_m}{K}, \quad (5)$$

where K is the equilibrium constant from above. Using this approach, k_m increases rapidly with temperature while k_f is temperature independent because the temperature dependence of k_m is compensated by the temperature dependence of K.

For a kinetic model it is necessary to pay attention to the details of the experimental method. We start by considering the experiments without the annealing section. In this configuration there is a cluster growth period after which the clusters travel, at a fixed temperature, through the extension. The clusters are heated as they grow because addition of an atom to a cluster adds its binding energy to the internal energy. The dissociation energies for aluminum clusters in the size regime examined here are around 300 kJ/mol.[44] Adding this energy to a 55 atom cluster at 300 K will raise its temperature to around 525 K (assuming a classical heat capacity).

The excess energy deposited during cluster growth is removed by collisions with the helium buffer gas. We assume that each collision removes an energy

$$E_{\text{rem}} = k_B(T_{\text{cluster}} - T_{\text{buffer}}), \quad (6)$$

where k_B is the Boltzmann constant and T_{cluster} and T_{buffer} are the temperatures of the cluster and the buffer gas, respectively. The cooling rate depends on the number of vibrational degrees of freedom in the cluster and the collision rate. With our experimental conditions, a 55-atom cluster with T_{cluster} = 600 K and T_{buffer} = 300 K cools exponentially to within 1 K of 300 K in around 1 μs, according to the model.

To simulate the experiments without the annealing section we start with hot liquid clusters and numerically integrate the rate equations for formation and loss of S_A, S_B, and L as the clusters cool according to Eq. (6). After the clusters are quenched, we fix the temperature and then integrate the rate equations for an additional 1.2 ms to simulate passage through the temperature variable extension. We use the same values for ΔH_m^A, ΔH_m^B, T_m^A, and T_m^B as used for the equilibrium model (see Table I). For both melting processes ($S_A \rightarrow L$ and $S_B \rightarrow L$) we employ a pre-exponential factor A in Eq. (4) of 10^{21} s^{-1}. The consequences of using different values are considered below.

RESULTS FOR THE KINETIC MODEL WITHOUT ANNEALING

The results on the left of Fig. 5 (color online) are for case 1 and those on the right are for case 2. The top panels show the rate constants determined from Eq. (4) and (5), as a function of temperature. As noted above, the rate constants for melting increase rapidly with temperature while those for freezing are temperature independent (according to the assumptions made above). The freezing and melting rate constants become equal at the melting temperature.

The panels second from the top in Fig. 5 show the abundances of solids A (green) and B (blue) and the liquid (red) as a function of temperature as the clusters are quenched from 1000 to 100 K. Similar results are obtained if we quench from 600 to 300 K. The liquid clusters freeze as the temperature is lowered. For case 1 (left side of Fig. 5) the clusters freeze at around 500 K into S_B. This freezing transition occurs close to the thermodynamic freezing temperature (500 K) because the freezing rate exceeds the cooling rate. If the cooling rate is larger than the freezing rate the clusters supercool and freeze below 500 K (see below).

Solid B is the thermodynamically preferred solid at the freezing temperature for case 1. As the temperature is lowered, S_A becomes thermodynamically preferred, and a solid-to-solid transition would occur at 286 K if the system behaved thermodynamically (as in Fig. 4). However, this transition does not happen on the timescale of the quenching process, and solid B persists below 286 K.

The third panels from the top in Fig. 5 show S_A (green), S_B (blue), and L (red) abundances that result after passage through the temperature variable extension. Here we have taken the abundances from the end of the quenching simulations and numerically integrated the rate equations at a fixed temperature for 1.2 ms (the average time the clusters spend traveling through the extension). These simulations are performed for temperatures from 100 to 1000 K in 10 K increments. The component of the heat capacities due to the latent heat is then determined using Eq. (3).

For case 1 (left side of Fig. 5) a melting transition occurs for S_B at 500 K. There is a corresponding peak in the heat capacities, shown in the bottom panel of the figure. The area under the peak is the latent heat for melting S_B (100 kJ/mol). There is no appreciable conversion of S_B to S_A below 286 K (where S_A is thermodynamically preferred) even on the much longer timescale for transit through the temperature variable extension. In our model it is necessary to go through the liquid state to convert S_B to S_A, and the melting rate for S_B at 286 K is small.

The panels on the right side of Fig. 5 show results for case 2. For case 2, solid A is thermodynamically preferred for all temperatures below the freezing temperature (see Fig. 4). During quenching, a small amount of S_A (green) is formed starting at around 500 K. However, the cooling rate is larger than the freezing rate for solid A so most of the liquid supercools to around 400 K where it freezes into solid B (blue). The liquid freezes into S_B instead of S_A because the freezing rate for S_B is larger than for S_A.

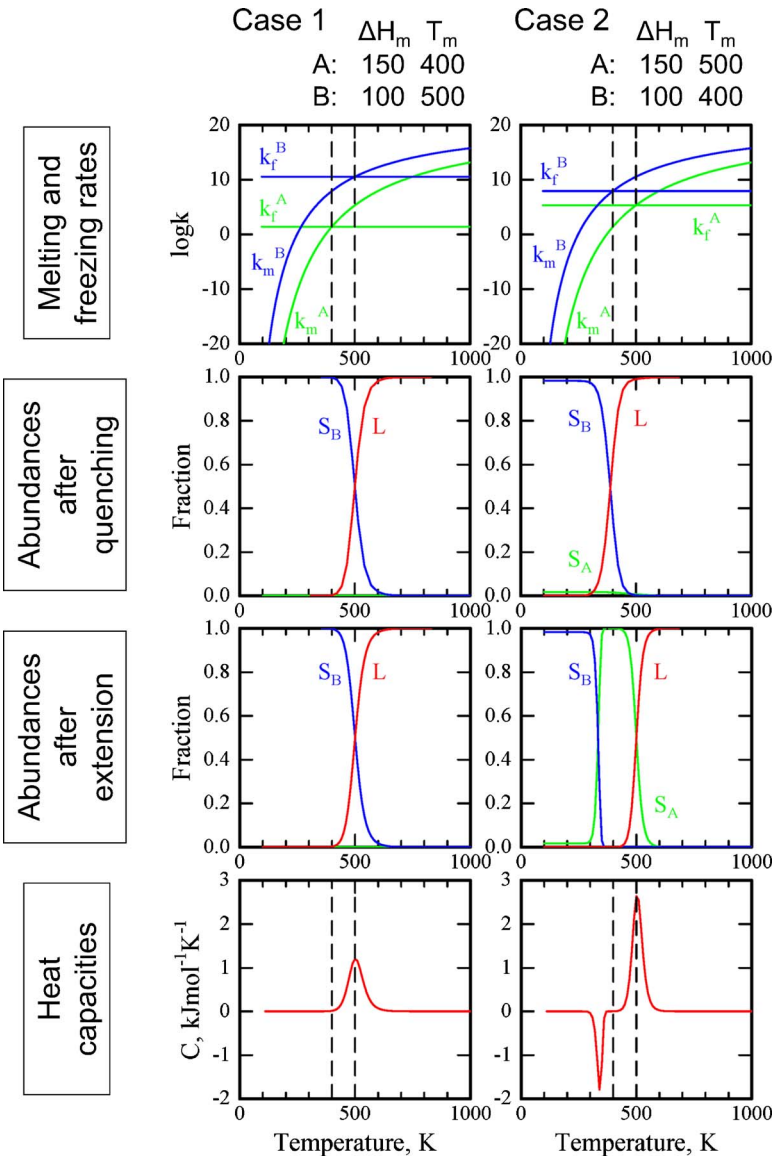

FIG. 5. (Color online) Predictions of the kinetic model. The panels on the left show results for case 1 and those on the right are for case 2. The top panels show rate constants for melting and freezing plotted against temperature. The panels second from the top show the abundances of solid A (green), solid B (blue), and liquid (red) as the clusters are quenched from 1000 to 100 K. The panels third from the top show the relative abundances after passing through the temperature variable extension (constant temperature for 1.2 ms). The bottom panels show the component of the heat capacities due to the latent heat.

The abundances after passage through the temperature variable extension for case 2 (Fig. 5, right side, third panel down) show a transition from S_B to S_A at around 360 K (below the melting temperatures of both solids). The transition occurs here, but not during quenching, because there is much more time available (1.2 ms compared to around 1 μs). The transition from S_B to S_A leads to a dip in the heat capacity (bottom panel in Fig. 5) because S_A is lower in energy than S_B. Thus, the kinetic model can account for the presence of the dips. At 500 K solid A melts. This process is accompanied by a peak in the heat capacity. The area under the peak is the latent heat of S_A (150 kJ/mol).

VARYING THE PRE-EXPONENTIAL FACTORS FOR CASE 2

Figure 6 shows the effect of varying the pre-exponential factors for case 2. The upper panels show the rate constants. An important quantity for comparison with the rate constants is the rate at which the clusters are quenched from 500 to 400 K. This is the reciprocal of the time it takes to cool between these temperatures. The upper dashed horizontal line in Fig. 6 shows the cooling rate. Freezing processes with rates significantly smaller than this cooling rate do not occur during quenching. The lower dashed horizontal line in Fig. 6 shows the reciprocal of the transit time through the temperature variable extension (10^3 s^{-1}). Comparison to this rate provides information about what processes can occur as the clusters travel through the extension.

The panels second from the top in Fig. 6 report the fractions of solid A (green), solid B (blue), and liquid (red) present during quenching from 1000 to 100 K. With pre-exponential factors of 10^{24} s^{-1}, the melting and freezing rates are large enough that the system remains in the thermodynamic limit during quenching and freezes into solid A. However, when the pre-exponential factors are reduced to 10^{23} s^{-1}, quenching no longer leads exclusively to the thermodynamically preferred solid and a significant amount of solid B is formed. This occurs because the freezing rate for solid A is comparable to the cooling rate and so some of the liquid supercools and bypasses freezing into solid A. As the

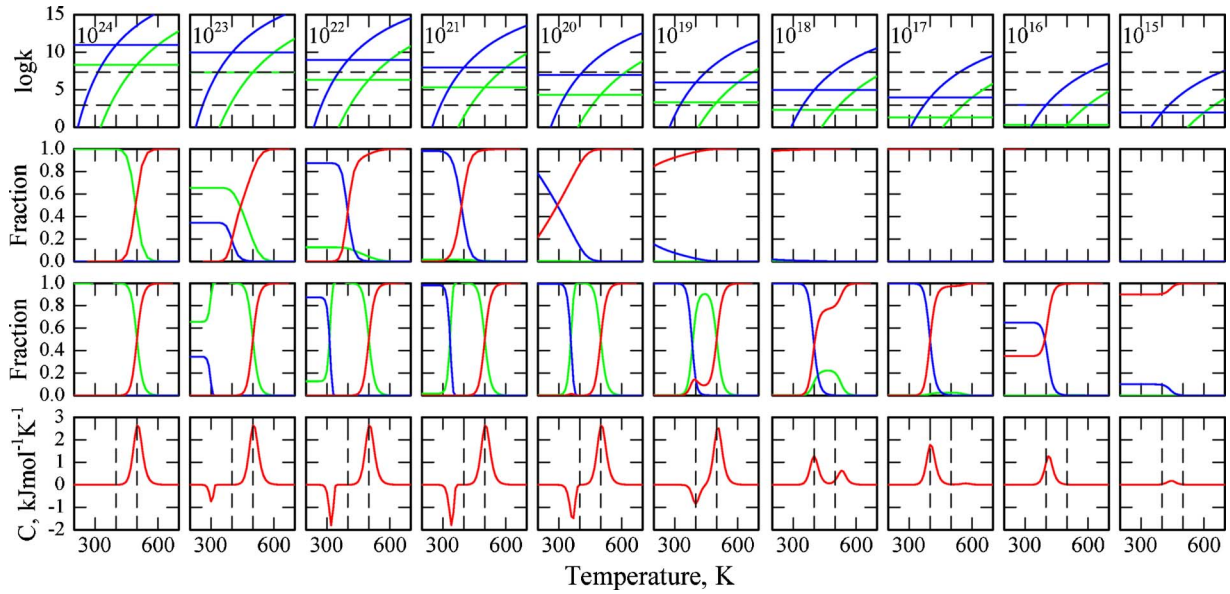

FIG. 6. (Color online) Predictions of the kinetic model for case 2 as a function of the pre-exponential factors (from 10^{24} to 10^{15} s^{-1}) in the Arrhenius expression for the melting rate constants. The upper panels show rate constants for melting and freezing: Green lines for solid A and blue lines for solid B. The panels second from the top show the relative abundances of solid A (green), solid B (blue), and liquid (red) as the clusters are quenched from 1000 to 100 K. The panels third from the top show the abundances after passing through the temperature variable extension (constant temperature for 1.2 ms). The bottom panels show the component of the heat capacities due to the latent heat.

pre-exponential factor is lowered further, the fraction of solid B formed during quenching increases and becomes dominant at 10^{21} s^{-1}.

With even smaller pre-exponential factors, the freezing rate for solid B decreases and becomes comparable to the cooling rate. The liquid then supercools and freezes at significantly below 400 K (see results in Fig. 6 for pre-exponential factors of 10^{20} s^{-1}). As the pre-exponential factor is lowered even further, the freezing rate decreases to the point where the liquid does not freeze during quenching.

The panels third from the top in Fig. 6 show the fractions of solid A (green), solid B (blue), and liquid (red) after passage through the temperature variable extension. With pre-exponential factors of 10^{24} s^{-1}, the freezing and melting rates are sufficiently large at all relevant temperatures that the clusters behave thermodynamically during quenching and in the temperature variable extension. Solid A is the thermodynamically preferred solid for case 2 and there is a single peak in the heat capacity (bottom panel in Fig. 6) at 500 K due to the melting of solid A.

As the pre-exponential factors are reduced, the dip in the heat capacities appears and becomes deeper as a larger fraction of solid B is trapped during quenching. In our model, annealing occurs through the liquid. The annealing temperature (the center of the dip in the heat capacities) is below both melting temperatures. However, below the melting temperature the clusters still spend a small fraction of their time in the liquid state. The clusters are mostly solid below the melting temperature because the freezing rate is larger than the melting rate. For annealing to occur, the melting rate for solid B must be large enough that it melts during transit through the temperature variable extension. With pre-exponential factors of 10^{23} s^{-1}, a temperature of around 300 K is required. As the pre-exponential factors decrease, the annealing temperatures increase because a higher temperature is needed to achieve the melting rates required for annealing. For 10^{19} s^{-1} the annealing temperature has risen to 400 K, the melting temperature of solid B.

The annealing process is not as straight forward as it appears at first glance. After solid B melts at the annealing temperature, it rapidly refreezes. The freezing rate to form solid B is much larger than to form solid A, so most of the melted solid B just refreezes back to solid B. However, a small amount freezes into solid A, and since the melting rate of solid A is much smaller than that of solid B, once solid A is formed it does not remelt to a significant extent. So at the annealing temperature, solid B is gradually syphoned off into solid A through many melting and refreezing cycles.

The freezing rates decrease with the pre-exponential factors and at 10^{19} s^{-1} the time scale for freezing into solid A is comparable to the transit time through the temperature variable extension. So instead of freezing into solid A some of the liquid now persists. With pre-exponential factors of 10^{18} s^{-1} the freezing rate for solid A is sufficiently small that when solid B melts, most of the liquid does not refreeze into solid A. The dip in the heat capacities that resulted from solid B converting into solid A is now replaced by a peak due to the melting of solid B. There is also a small peak at higher temperature due to the melting of solid A. This peak is diminished because only a small amount of solid A remains to melt. Note also that the peak occurs significantly above 500 K. The clusters superheat because the melting rate at the melting temperature is too small for all of the clusters to melt in the extension.

For pre-exponential factors of 10^{17} s^{-1} essentially all of solid B melts directly instead of annealing into solid A and there is a single dominant peak in the heat capacity at 400 K. For pre-exponential factors of 10^{16} s^{-1} and smaller, the freez-

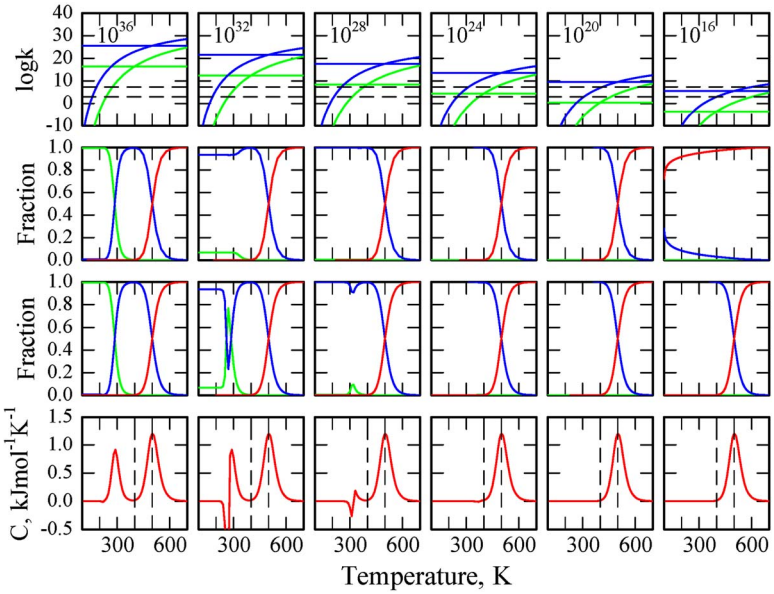

FIG. 7. (Color online) Predictions of the kinetic model for case 1 as a function of the pre-exponential factors (from 10^{36} to 10^{16} s^{-1}) in the Arrhenius expression for the melting rate constants. The top panels show rate constants for melting and freezing: Green lines for solid A and blue lines for solid B. The panels second from the top show the relative abundances of solid A (green), solid B (blue), and liquid (red) as the clusters are quenched from 1000 to 100 K. The panels third from the top show the abundances after passing through the temperature variable extension (constant temperature for 1.2 ms). The bottom panels show the component of the heat capacities due to the latent heat.

ing rates have now decreased to the point that the clusters do not fully freeze as they travel through the temperature variable extension and so the size of the peak in the heat capacity becomes smaller and it eventually vanishes as more of the clusters remain liquid (they do not freeze on the timescale of the experiment).

VARYING THE PRE-EXPONENTIAL FACTORS FOR CASE 1

The effects of varying the pre-exponential factors on the melting and freezing behavior for case 1 are shown in Fig. 7. Solid B is thermodynamically preferred for $T>286$ K. The clusters always freeze into solid B during quenching, even when they supercool, because solid B has a larger freezing rate than solid A. The heat capacities for pre-exponential factors of 10^{24}–10^{16} s^{-1} show a single peak at 500 K due to melting of solid B. For pre-exponential factors smaller than 10^{16} s^{-1}, the peak in the heat capacity eventually disappears as the freezing rate decreases and the clusters remain liquid during passage through the extension.

With the values of ΔH_m and T_m used here, pre-exponential factors greater than 10^{24} s^{-1} yield freezing times that are unrealistically short (shorter than a vibrational period). We include these results in Fig. 7 to show the transition to thermodynamic behavior. With pre-exponential factors of 10^{36} s^{-1}, the system behaves thermodynamically and there are two peaks in the heat capacities resulting from melting at 500 K and the solid-to-solid transition at 286 K. As the pre-exponential factor is decreased, kinetics takes over. A sharp dip emerges in the heat capacities obtained with pre-exponential factors of 10^{32} and 10^{28} s^{-1}, which results from solid B that is trapped during quenching and starts to anneal into solid A just before the solid-to-solid transition. The solid-to-solid transition is not observed with pre-exponential factors of 10^{24} s^{-1} and smaller.

INCORPORATING THE ANNEALING SECTION INTO THE SIMULATIONS

With the annealing section the sequence of events is (1) quench from 1000 K to the annealing temperature as described above; (2) hold the temperature at the annealing temperature for 0.6 ms (the average transit time through the annealing section in the experiments); (3) make a linear transition between the temperature of the annealing section and the temperature of the extension over 0.12 ms (the average transit time through the Macor® spacer that separates the annealing section from the temperature variable extension); and (4) keep the temperature fixed for 1.2 ms as the clusters travel through temperature variable extension. We numerically integrate the rate equations for creation and destruction of S_A, S_B, and L through these four steps. Some results from these simulations are shown in Fig. 8 for case 2 with pre-exponential factors of 10^{23}–10^{18} s^{-1}. The top panels show the heat capacities due to the latent heat obtained without the annealing section. Dips occur for pre-exponential factors of 10^{23}–10^{19} s^{-1}, while for 10^{18} s^{-1} there are two peaks.

The panels second from the top in Fig. 8 show heat capacities due to the latent heat obtained with the annealing section at 800 K (which is above both melting temperatures). The dip essentially disappears for pre-exponential factors of 10^{23}–10^{21} s^{-1} and it is significantly diminished for 10^{20} s^{-1}. For pre-exponential factors of 10^{19} s^{-1} the dip is unchanged by annealing to 800 K and for 10^{18} s^{-1}, the two peaks in the heat capacity are unchanged.

The panels third from the top and at the bottom in Fig. 8 show results obtained with the annealing temperature set to 500 and 400 K, respectively (we do not show plots for pre-exponential factors of 10^{23} and 10^{22} s^{-1} because the dips disappeared at 800 K). For pre-exponential factors of 10^{20} s^{-1} the dip is diminished with an annealing temperature of 500 K and disappears with an annealing temperature of 400 K. With pre-exponential factors of 10^{19} s^{-1} the dip is diminished but does not disappear. For 10^{18} s^{-1} the two

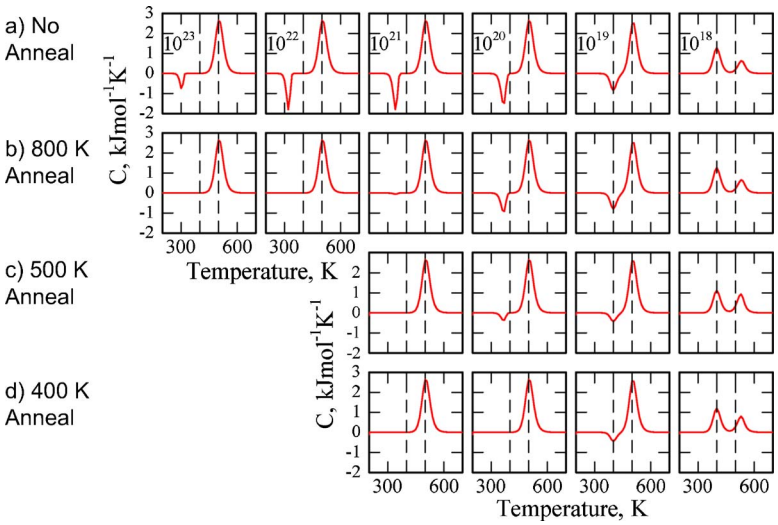

FIG. 8. (Color online) Effect of annealing on the component of the heat capacities due to the latent heat for case 2. Results are shown for pre-exponential factors from 10^{23} to 10^{18} s^{-1}. The upper panels (a) show heat capacities obtained from the simulations without the annealing section (as in Fig. 6). The results in the panels second from the top (b) were obtained with the annealing section at 800 K. The results in the panels that are third from the top (c) and at the bottom (d) were obtained with annealing temperatures of 500 and 400 K, respectively.

peaks remain in the heat capacities although their relative abundances are slightly altered with the gentler annealing conditions.

In summary, the simulations that incorporate the annealing section reproduce the main features of the experimental results, including the observations that some of the dips disappear when the clusters are annealed, more dips disappear with the milder annealing conditions, and that some of the dips do not disappear.

DISCUSSION

In our model, the melting rates are given by the Arrhenius expression where we use the latent heat as the activation energy. This leads to freezing rates that are temperature independent. For a macroscopic liquid, freezing occurs through the formation of a critical nucleus and its rate of formation is expected to increase as the temperature drops. This behavior was observed, for example, by Chushak and Bartell in molecular dynamics simulations of the freezing of gold nanoclusters with 459, 1157, and 3943 atoms.[45] Since the clusters studied here are much smaller, the freezing mechanisms are expected to be different. It is not known if the freezing rates for metal clusters increase with decreasing temperature. However, a temperature dependent freezing rate should not affect our main conclusions, because in the dynamic coexistence regime the temperature dependences of the melting and freezing rates are coupled.

The dips in the heat capacities result from freezing into a high energy geometry. For this to occur (1) the freezing rate for the high energy geometry must be larger than for the thermodynamically preferred and (2) the freezing rate for the thermodynamically preferred solid must be less than the cooling rate. If these conditions are met, the liquid will bypass freezing into the thermodynamically preferred solid (which always has the higher freezing temperature) and freeze into the higher energy geometry at a lower temperature. This starts to occur in the simulations for case 2 when the freezing rate constant for the thermodynamically preferred solid (green horizontal lines in the top panels of Fig. 6) becomes $<10^8$ s^{-1}.

The dip results because the higher energy geometry that is trapped during quenching converts into the thermodynamically preferred solid during transit through the temperature variable extension. This transition occurs because it takes much longer to travel through the extension than to quench the clusters (1.2 ms versus around 1 μs).

Conversion of the high energy geometry to the thermodynamically preferred solid occurs through the liquid in our model (i.e., by melting and refreezing). When the time scale for freezing into the thermodynamically preferred solid becomes greater than the transit time through the temperature variable extension, the liquid no longer refreezes, and the dip is replaced by a second peak in the heat capacities (due to melting of the high energy solid). This occurs when the freezing rate for thermodynamically preferred solid becomes $<10^3$ s^{-1} (see Fig. 6).

We normally attribute heat capacity plots with two peaks to premelting phenomena (such as surface premelting[46–52]). The simulations reported here show that when the freezing rate for the thermodynamically preferred solid is small, the melting of two different solid states with different melting temperatures can also lead to two peaks in the heat capacities.

The dips disappear when the clusters are annealed because the cooling rate is decreased. The hot clusters generated during cluster growth are quenched in $\sim$1 μs. However, the hot clusters generated by annealing are cooled in $\sim$100 μs. Fewer clusters are trapped in the high energy structure with the lower cooling rate. The cooling rates are lowered further with the milder annealing conditions and more of the dips disappear.

The parameter that determines whether or not the dips disappear is the freezing rate for the thermodynamically preferred solid. From inspection of Figs. 6 and 8, we can deduce the values required to account for the experimental observations. For clusters where the dip disappears upon annealing to $>$800 K the freezing rate into the thermodynamically preferred solid (green horizontal lines in the top panels of Fig. 6) must fall in the 10^8–10^5 s^{-1} range, and when the dip persists after annealing to $>$800 K the freezing rate must fall in the 10^4–10^3 s^{-1} range.

Finally, we have not yet considered the nature of the high energy geometry that the clusters can freeze into at high cooling rates. One obvious candidate is a glassy or amorphous structure. Glasses are known to form at high cooling rates. During quenching, the cooling rates between 400 and 500 K are in the 10^9 K s^{-1} range while for the mildest annealing conditions the cooling rate is around 10^6 K s^{-1}. However, single component metals are notoriously poor glass formers and much higher cooling rates (10^{14} K s^{-1}) appear necessary to generate glassy clusters.[53]

CONCLUSIONS

Annealing studies indicate that the dips in the heat capacities of some aluminum cluster cations do not result from amorphous or badly formed geometries generated during cluster growth. To investigate the origin of the dips we developed a simple kinetic model of melting and freezing in a system consisting of one liquidlike and two solidlike states with different latent heats and melting temperatures.

The simulations show that a variety of heat capacity signatures are possible depending on the freezing and melting rates. The model is able to account for the existence of the dips in the heat capacities, the fact that some of the dips are annealed away while others are not, and the dependence on the annealing temperature.

The simulations indicate that the dips result from preferential freezing into a high energy geometry and then conversion into the thermodynamically preferred solid during transit through the temperature variable extension. While the thermodynamically preferred solid has the highest freezing temperature, the liquid can bypass the thermodynamically preferred solid and freeze into a higher energy geometry if it has a higher freezing rate.

ACKNOWLEDGMENTS

We gratefully acknowledge the support of the National Science Foundation.

[1] P. Z. Pawlow, Z. Phys. Chem., Stoechiom. Verwandtschaftsl. **65**, 1 (1909).
[2] M. Takagi, J. Phys. Soc. Jpn. **9**, 359 (1954).
[3] S. J. Peppiatt, Proc. R. Soc. London, Ser. A **345**, 401 (1975).
[4] Ph. Buffat and J. P. Borell, Phys. Rev. A **13**, 2287 (1976).
[5] P. R. Couchman and W. A. Jesser, Nature (London) **269**, 481 (1977).
[6] S. L. Lai, J. Y. Guo, V. Petrova, G. Ramanath, and L. H. Allen, Phys. Rev. Lett. **77**, 99 (1996).
[7] M. Schmidt, R. Kusche, W. Kronmüller, B. von Issendorf, and H. Haberland, Phys. Rev. Lett. **79**, 99 (1997).
[8] M. Schmidt, R. Kusche, B. von Issendorf, and H. Haberland, Nature (London) **393**, 238 (1998).
[9] M. Schmidt and H. Haberland, C. R. Phys. **3**, 327 (2002).
[10] M. Schmidt, J. Donges, Th. Hippler, and H. Haberland, Phys. Rev. Lett. **90**, 103401 (2003).
[11] A. A. Shvartsburg and M. F. Jarrold, Phys. Rev. Lett. **85**, 2530 (2000).
[12] G. A. Breaux, R. C. Benirschke, T. Sugai, B. S. Kinnear, and M. F. Jarrold, Phys. Rev. Lett. **91**, 215508 (2003).
[13] G. A. Breaux, D. A. Hillman, C. M. Neal, R. C. Benirschke, and M. F. Jarrold, J. Am. Chem. Soc. **126**, 8628 (2004).
[14] K. Joshi, D. G. Kanhere, and S. A. Blundell, Phys. Rev. B **66**, 155329 (2002).
[15] K. Joshi, D. G. Kanhere, and S. A. Blundell, Phys. Rev. B **67**, 235413 (2003).
[16] S. Chacko, K. Joshi, and D. G. Kanhere, Phys. Rev. Lett. **92**, 135506 (2004).
[17] F.-C. Chuang, C. Z. Wang, S. Öğüt, J. R. Chelikowsky, and K. M. Ho, Phys. Rev. B **69**, 165408 (2004).
[18] K. Manninen, A. Rytkönen, and M. Manninen, Eur. J. Phys. **29**, 39 (2004).
[19] S. Chacko, D. G. Kanhere, and S. A. Blundell, Phys. Rev. B **71**, 155407 (2005).
[20] A. Aguado and J. M. Lopez, Phys. Rev. Lett. **94**, 233401 (2005).
[21] S. Krishnamurty, S. Chacko, D. G. Kanhere, G. A. Breaux, C. M. Neal, and M. F. Jarrold, Phys. Rev. B **73**, 045406 (2006).
[22] K. Joshi, S. Krishnamurty, and D. G. Kanhere, Phys. Rev. Lett. **96**, 135703 (2006).
[23] E. G. Noya, J. P. K. Doye, and F. Calvo, Phys. Rev. B **73**, 125407 (2006).
[24] W. Zhang, F. Zhang, and Z. Zhu, Phys. Rev. B **74**, 033412 (2006).
[25] A. Aguado and J. M. Lopez, J. Phys. Chem. B **110**, 14020 (2006).
[26] A. Aguado and J. M. Lopez, Phys. Rev. B **74**, 115403 (2006).
[27] G. A. Breaux, C. M. Neal, B. Cao, and M. F. Jarrold, Phys. Rev. Lett. **94**, 173401 (2005).
[28] C. M. Neal, A. K. Starace, and M. F. Jarrold, Phys. Rev. B **76**, 054113 (2007).
[29] C. M. Neal, A. K. Starace, and M. F. Jarrold, J. Am. Soc. Mass Spectrom. **18**, 74 (2007).
[30] C. M. Neal, G. A. Breaux, B. Cao, A. K. Starace, and M. F. Jarrold, Rev. Sci. Instrum. **78**, 075108 (2007).
[31] M. F. Jarrold and E. C. Honea, J. Phys. Chem. **95**, 9181 (1991).
[32] M. F. Jarrold and E. C. Honea, J. Am. Chem. Soc. **114**, 459 (1992).
[33] J. Bohr, Int. J. Quantum Chem. **84**, 249 (2001).
[34] R. S. Berry, J. Jellinek, and G. Natanson, Phys. Rev. A **30**, 919 (1984).
[35] T. L. Beck, J. Jellinek, and R. S. Berry, J. Chem. Phys. **87**, 545 (1987).
[36] J. P. Rose and R. S. Berry, J. Chem. Phys. **98**, 3246 (1993).
[37] B. Vekhter and R. S. Berry, J. Chem. Phys. **106**, 6456 (1997).
[38] C. L. Cleveland, U. Landman, and W. D. Luedtke, J. Phys. Chem. **98**, 6272 (1994).
[39] C. L. Cleveland, W. D. Luedtke, and U. Landman, Phys. Rev. B **60**, 5065 (1999).
[40] S. C. Hendy, Phys. Rev. B **71**, 115404 (2005).
[41] D. Schebarchov and S. C. Hendy, J. Chem. Phys. **123**, 104701 (2005).
[42] J. P. K. Doye and D. J. Wales, Phys. Rev. Lett. **80**, 1357 (1998).
[43] D. Poland, J. Chem. Phys. **126**, 054507 (2007).
[44] A. K. Starace, C. M. Neal, B. Cao, M. F. Jarrold, A. Aguado, and J. M. López (unpublished).
[45] Y. G. Chushak and L. S. Bartell, J. Phys. Chem. B **105**, 11605 (2001).
[46] V. V. Nauchitel and A. J. Pertsin, Mol. Phys. **40**, 1341 (1980).
[47] H.-P. Cheng and R. S. Berry, Phys. Rev. A **45**, 7969 (1992).
[48] A. Aguado, J. M. Lopez, J. A. Alonso, and M. J. Stott, J. Chem. Phys. **111**, 6026 (1999).
[49] F. Calvo and F. Spiegelmann, J. Chem. Phys. **112**, 2888 (2000).
[50] Y. J. Lee, E.-K. Lee, and S. Kim, Phys. Rev. Lett. **86**, 999 (2001).
[51] A. Aguado, L. M. Molina, J. M. Loez, and J. A. Alonso, Eur. Phys. J. D **15**, 221 (2001).
[52] F. Calvo and F. Spiegelmann, J. Chem. Phys. **120**, 9684 (2004).
[53] H.-P. Cheng and U. Landman, J. Phys. Chem. **98**, 3527 (1994).